Contemporary Mathematics
http://ojs.wiserpub.com/index.php/CM/

Research Article

Mathematical Modeling on Weakened Thermomagnetic Nanobeam Based on the Nonlocal Strain Gradient Theory

Mohammadreza Eghbali[1], Seyed Amirhosein Hosseini[2*], Mahdi Keshtkar[2]

[1] Department of Mechanical Engineering, University of Zanjan, Zanjan, Iran
[2] Buein Zahra Technical University, Buein Zahra, Qazvin, Iran
E-mail: amirh12211@gmail.com

Received: 30 March 2023; **Revised:** 24 July 2023; **Accepted:** 25 April 2024

Abstract: In this research paper, the focus is on analyzing the free lateral vibration of a nanobeam that has been weakened. The investigation revolves around studying the impact of thermal and magnetic effects on the nanobeam, utilizing both Bernoulli's beam theory and the nonlocal strain gradient theory (NSGT). Nanostructures hold great significance and find various applications. To derive the governing equations, boundary conditions, and assess the thermal and magnetic influences, Hamilton's principle is employed. The nanobeam is divided into two parts, with rotational springs connecting them. This model takes into account the additional strain energy caused by cracks, which in turn increases the deflection slope's discontinuity. The study examines various factors such as crack propagation, crack intensity, thermal and magnetic effects, material length scale parameters, and nonlocal parameters within the non-rheological parameters. A comparative analysis with previous research studies has been conducted, demonstrating a favorable agreement between the findings. The results highlight the significant role played by the aforementioned parameters in the dynamic behavior of the nanobeam. Also, the location and severity of the crack on the nanobeam and its effect on the free vibrations were investigated. The most important application of the conducted research can be used in the construction of drug release systems and stimulate the drugs in a controlled and direct manner at the target site.

***Keywords*:** nanobeam, nonlocal strain gradient theory, vibration analysis, crack, thermo-magneto effects

MSC: 65L05, 34K06, 34K28

1. Introduction

Today, the application of nanotechnology in drug delivery and the treatment of some diseases has become an attractive and promising path. In this regard, and with the proliferation of nano-sensors, the field of pathogen detection to prevent the spread of epidemics is also being realized. In fact, pathogens such as viruses and bacteria have unique effects on nano-sensors based on their different mass and structure. One of these effects is a change in the vibrational frequency of the nano-sensors. Therefore, due to the widespread use of this type of structure in modern technology, the importance of studying the vibrations of this type of structure is of great importance [1–7].

Wang et al. analyzed the vibrations of porous Timoshenko beams in a hygrothermal environment. The equations were extracted by Hamilton's principle and the nonlinear strain gradient theory and solved by the GDQ numerical method. The

DOI: https://doi.org/10.37256/cm.6120252762

effect of different parameters on the mechanical behavior of nanobeam is investigated [8]. Thai et al. analyzed composite layered nanoplates with free and static vibrations with a classical higher-order shear deformation theory dependent on size effects. The equations are derived using nonlocal theory and strain gradient. The results are compared with numerical studies and examined for different parameters [9]. Malikan et al. studied torsional stability of a single-walled composite nano-shell (SWCNS) under a three-dimensional magnetic field. The analysis utilized a nonlocal model and the first-order shear deformation shell theory (FSDST) [10].

Merzouki et al. studied the buckling of an FG porous nanobeam reinforced with graphene platelets. Relationships are extracted using nonlocal strain gradient theory and bivariate shear deformation theory. The governing equations are solved by introducing a three-node beam element. Moreover, the effect of various factors on the mechanical behavior of the structure, including graphene reinforcement, has been studied [11]. Tho et al. introduced a novel approach by combining the finite element method (FEM) with a third-order shear deformation beam theory (TSDT) to simulate the static bending and free vibration responses of piezoelectric nanobeams with geometric imperfections [12]. Duc et al. presented novel numerical findings on the analysis of vibration response in a cracked functionally graded material (FGM) plate, utilizing the phase-field theory and finite element method [13]. Dung et al. investigated an analysis of the static bending behavior of microplates placed on imperfect elastic foundations using a nonlinear approach. The finite element method, incorporating the modified couple stress theory, were employed to establish the nonlinear finite element equations [14]. Tho et al. employd the third-order shear deformation theory along with the phase-field theory to simulate the free vibration response and static bending of laminated composite plates that exhibit a fracture in the core layer only [15]. Khan et al. investigated Hall current effect, entropy generation, Arrhenius activation energy, and binary chemical reactions in heat and mass transfer bioconvection flow of Maxwell nanofluid [16]. Ramazan et al. investigated the mechanical properties of heat and mass transfer in a nanofluid of second grade, combined with the motion of gyrotatic microorganisms around a thin needle that exhibits a dipole effect [17]. Khan et al. presented an analytical analysis of the flow characteristics of a two-dimensional hybrid nanofluid [18].

Li et al. investigated the buckling behavior of functionally graded nanotubes whose material properties are different in two directions. The equations were extracted using the von-Kármán nonlinear theory and energy method, using the nonlocal strain gradient theory, and solved using the GDQ method [19]. Malikan et al. developed the first-order shear deformation theory (OVFSDT), to analyze the stability of a piezo-magnetoelectric composite nanoplate (PMEN). Equilibrium equations were formulated using a nonlocal strain gradient theory, and numerical results were obtained using analytical approaches. This study, offered advantages over conventional theories, such as no need for shear correction factors and fewer unknowns [20].

Forooghi et al. investigated the vibrational behavior of nanobeam reinforced with carbon nanotubes. The relationships were extracted using higher-order shear deformation theory and nonlocal strain gradient theory and solved by GDQ numerical method. Nano-beam is located in the hygrothermal and magnetic environment, and these factors' effect on nanobeam vibrations has been investigated [21]. Khan et al. studied the magnetic dipole effect on a thixotropic nanofluid flowing through a porous medium over a curved stretching surface, taking into account heat and mass transfer, as well as microorganism concentration [22].

Eftekhari et al. investigated the dynamic behavior of composite nanobeam with piezoelectric layers. The equations were extracted using the NSGT and solved by the GDQ method. Finally, the effect of various parameters, including surface effects, was investigated [23].

Malikan et al. analysed the forced vibration of single-walled carbon nanotubes using a new shear deformation beam theory. The theory considered nonlocal strain gradient effects and eliminated the need for shear correction factors. The study explored the effects of various parameters on the nanotubes' dynamic vibration [24]. Khan et al. studied the examination of entropy generation in an unsteady flow of Casson nanofluid, which includes gyrotactic microorganisms and is subject to the Cattaneo-Christov theory of heat and mass flux [25].

Rajaei et al. investigated the adaptive self-organizing fuzzy sliding mode controller for a nonlocal strain gradient nanobeam [26]. Rajaei et al. investigated the size-dependent differential quadrature element model for vibration analysis of FG CNT reinforced composite micro rods based on the higher-order Love-Bishop rod model and the nonlocal strain gradient theory [27]. Cuong-Le et al. investigated the nonlocal strain gradient numerical solution for static bending, free

vibration, and buckling of sigmoid FG sandwich nanoplate [28]. Malikan et al. studied the dynamic response of curved viscoelastic carbon nanotubes. They addressed the challenge of understanding the mechanical behavior of these curved nanotubes with the influence of material viscosity. The Kelvin-Voigt viscoelastic model and a modified shear deformation beam theory were used to formulate the governing equations [29]. Khan et al. examined the effects of magnetic fields and thermal radiation on homogeneous-heterogeneous chemical reactions involving second-grade nanofluid and gyrotactic microorganisms in a rotating system [30].

Yang et al. presented a nanobeam model that incorporates various high-order shear deformation beam theories. The model investigates the vibration response of nanobeams by considering two-phase local/nonlocal strain and stress gradient theory, along with surface elasticity theory [31]. Qing et al. presented a new mathematical formulation to address the stress-driven two-phase local/nonlocal integral model (SD-TPNIM) that incorporates discontinuity and symmetrical conditions [32]. Barretta et al. studied Nonlocal continuum theories within the context of nanobeams mechanics, specifically focusing on non-smooth fields which represent the most general condition [33]. Scorza et al. expanded the existing two-phase local/nonlocal stress-driven integral model (SDM) to include nanobeams with internal discontinuities [34]. Khan et al. investigated the Buongiorno nanofluid model, which considers the Cattaneo-Christov theory of heat and mass flux [35].

Su et al. investigated the vibration analysis of FG porous piezoelectric deeply curved beams resting on discrete elastic supports [36]. Arefi et al. studied the influence of flexoelectric surface and residual stress on the nonlinear vibration of sigmoid, exponential FG Timoshenko nano-beams [37]. Malikan et al. analysed the forced vibrations of a piezoelectric-piezomagnetic ceramic nanoplate using a refined shear deformation plate theory combined with a higher-order nonlocal strain gradient theory. The governing equations for the nanoplate were derived, considering stress nonlocality and strain gradient size-dependent effects [38]. Darban et al. developed a nonlocal approach to investigate the vibrations of nanobeams with varying sizes, considering the presence of cracks [39]. Khan et al. explored the impact of magnetic dipole, porosity, and heat transfer on the flow of a ferromagnetic Walter-B fluid over a curved stretching surface [40].

Bouafia et al. investigated the nonlocal quasi-3D theory for vibration behaviors of FG nanobeams [41]. Yahia et al. investigated the wave propagation in functionally graded plates with porosities using various higher-order plate theories [42]. Malikan et al. investigated the stability of a porous nanobeam under axial loading, considering flexomagnetic material properties [43]. Karami et al. investigated the resonance behavior of Kirchhoff nanoplates using the bi-Helmholtz nonlocal strain gradient theory [44].

Chaht et al. investigated size-dependent nanoscale beams' buckling analyses, including the thickness stretching effect [45]. Belkorissat et al. investigated the vibration properties of FG nanoplate using a new nonlocal refined four-variable model [46].

In this paper, the aim of investigating the free vibration of cracked nanoparticles using strain gradient theory considers thermal and magnetic effects. The crack beam is attached to the two sections connected with a circular spring in the crack position. Natural frequencies for cracked nanoparticles have been studied by applying boundary conditions and numerical results for different crack propagation, crack intensity, thermal and magnetic effects, the scale of material length, and different nonlocal parameters were investigated.

2. Formulation

Higher-order NSGT [47, 48] stress includes the nonlocal elastic and the strain gradient stress field.

$$t_{xx} = \sigma_{xx} - \nabla\sigma_{xx}^{(1)} \tag{1}$$

In Equation (1), σ_{xx} and $\sigma_{xx}^{(1)}$ the classical stresses and higher-order stresses, respectively, are shown in Equation (2) [48, 49]:

$$\sigma_{xx} = \int_0^L E(x)\alpha_0(x, x', e_0a)\varepsilon'_{xx}(x')dx'$$
$$\sigma_{xx}^{(1)} = l^2 \int_0^L E(x)\alpha_1(x, x', e_1a)\varepsilon'_{xx,x}(x')dx' \tag{2}$$

To investigate the importance of the nonlocal elasticity stress field, parameters e_0a and e_1a (which represent nonlocal parameters in Equation (2) e_0a and e_1a, are assumed in this study to be $e = e_0 = e_1$) and the characteristic parameter of materials l (which is also a parameter of the material length scale). It is presented to provide the strain gradient stress field [48]. In Equation (2) $\alpha(x, x', ea)$, the kernel function is nonlocal [47]. So the result is:

$$(1 - (ea)^2\nabla^2)\sigma_{xx} = E(x)\varepsilon_{xx} \tag{3}$$

$$(1 - (ea)^2\nabla^2)\sigma_{xx}^{(1)} = l^2E(x)\varepsilon_{xx,x} \tag{4}$$

where in Equations (1), (3) and (4) $\nabla = \dfrac{\partial}{\partial x}$. Using Equations (1), (3) and (4), (5) is achieved:

$$\left[1 - (ea)^2\nabla^2\right]t_{xx} = E(x)\varepsilon_{xx} - l^2\nabla.(E(x)\nabla\varepsilon_{xx}) \tag{5}$$

A nanobeam has width B, height h, and length L, as shown in Figure 1. Nanobeam has a torque modeled with a rotating spring in the crack position. This nanobeam is subject to the effects of thermal and magnetic effects.

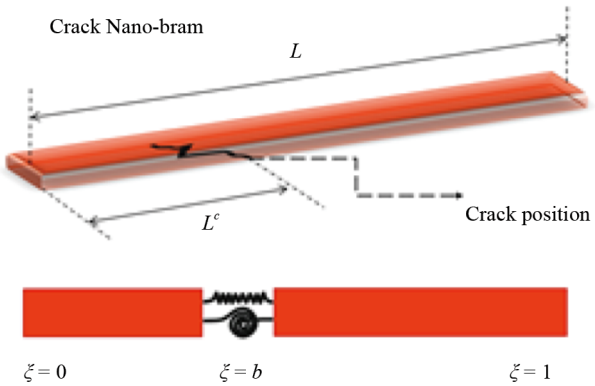

Figure 1. Schematic of a cracked beam

Free transverse vibration is considered a nanobeam. According to Euler Bernoulli's beam theory, the displacement field at any point in the arrow along its axis can be expressed as follows [49]:

$$u_1(x, z, t) = u(x, t) - zw_{,x}$$

$$u_2(x, z, t) = 0 \tag{6}$$

$$u_3(x, z, t) = w(x, t)$$

In the Euler Bernoulli beam, the longitudinal displacement of the center plate $u(x, t)$ is neglected due to its small size, so only the non-zero strain is expressed as follows:

$$\varepsilon_{xx} = u_{,x} - zw_{,xx} = -zw_{,xx} \tag{7}$$

Using Hamilton's principle, we have [48, 49]:

$$\int_{t_1}^{t_2} (\delta K - \delta U + \delta F_{EX.}) dt = 0 \tag{8}$$

$$\begin{aligned} \delta U &= \int_V (\sigma_{xx} \delta \varepsilon_{xx} + \sigma_{xx}^{(1)} \nabla \delta \varepsilon_{xx}) dV \\ &= \int_V (\sigma_{xx} - \nabla \sigma_{xx}^{(1)}) \delta \varepsilon_{xx} dV + \left[\int_A \sigma_{xx}^{(1)} \delta \varepsilon_{xx} dA \right]_0^L \\ &= \int_V t_{xx} \delta \varepsilon_{xx} dV + \left[\int_A \sigma_{xx}^{(1)} \delta \varepsilon_{xx} dA \right]_0^L \end{aligned} \tag{9}$$

The stress results are as follows:

$$\begin{aligned} M &= \int_A z t_{xx} dA \\ M^{(1)} &= \int_A z \sigma_{xx}^{(1)} dA \\ N_{xx} &= \int_A t_{xx} dA \\ N_{xx}^{(1)} &= \int_A \sigma_{xx}^{(1)} dA \end{aligned} \tag{10}$$

where in Equation (10), M the classical moment $M^{(1)}$ is the non-classical moment, N_{xx} and $N_{xx}^{(1)}$ the classical and non-classical force results. Due to the above relations:

$$\delta U = \int_0^L \left(N_{xx}\delta\frac{\partial u}{\partial x} - M\delta\frac{\partial^2 w}{\partial x^2}\right)dx + \left[N_{xx}^{(1)}\delta\frac{\partial u}{\partial x} - M^{(1)}\delta\frac{\partial^2 w}{\partial x^2}\right]_0^L$$

$$\delta K = \int_V \rho(x)\frac{\partial u_1}{\partial t}\delta\left(\frac{\partial u_1}{\partial t}\right)dV + \int_V \rho(x)\frac{\partial u_3}{\partial t}\delta\left(\frac{\partial u_3}{\partial t}\right)dV$$

$$= \int_0^L \rho(x)A\frac{\partial u}{\partial t}\delta\left(\frac{\partial u}{\partial t}\right)dx + \int_0^L \rho(x)I\frac{\partial^2 w}{\partial x\partial t}\delta\left(\frac{\partial^2 w}{\partial x\partial t}\right)dx \tag{11}$$

$$+ \int_0^L \rho(x)A\frac{\partial w}{\partial t}\delta\left(\frac{\partial w}{\partial t}\right)dx$$

$$\delta F_{EX.} = \int_0^L (N_T + N_M)\left(\frac{\partial w}{\partial x}\right)\delta\left(\frac{\partial w}{\partial x}\right)dx$$

In Equation (11), N_M and N_T denote a uniaxial magnetic field, thermal load caused by temperature change. The moment of inertia is as follows:

$$\left\{ \begin{array}{c} A \\ I \end{array} \right\} = b\int_{-\frac{h}{2}}^{\frac{h}{2}} \left\{ \begin{array}{c} 1 \\ z^2 \end{array} \right\} dz \tag{12}$$

Using Equations (11) and (8), solving the relationship and factorization:

$$\delta U = \frac{\partial N_{xx}}{\partial x} = 0$$

$$\delta w\text{: } \frac{\partial^2 M}{\partial x^2} + \frac{\partial}{\partial x}\left(\rho(x)I\frac{\partial^3 w}{\partial x\partial t^2}\right) - \rho(x)A\frac{\partial^2 w}{\partial t^2} - (N_T + N_M)\frac{\partial^2 w}{\partial x^2} = 0$$

$$B.C \Rightarrow \left[\begin{array}{l} N_{xx} = 0 \\ \\ \dfrac{\partial M}{\partial x} \text{ or } \delta w \\ \\ (N_T + N_M)\left(\dfrac{\partial w}{\partial x}\right) \end{array} \right]_{x\,=\,0,L} , \quad \left\{ \begin{array}{l} M = 0 \\ \\ N_{xx}^{(1)} \\ \\ M^{(1)} \text{ or } \dfrac{\partial^2 w}{\partial x^2} \end{array} \right. \tag{13}$$

Using Equations (5), (7), and (10):

$$M = (ea)^2 M_{,xx} - E(x)Iw_{,xx} + l^2 I\frac{\partial}{\partial x}(E(x)w_{,xxx}) \tag{14}$$

which in Equation (14), E is the modulus of elasticity and I is the moment of inertia. Using Equations (13) and (14):

$$M = (ea)^2 \left[\rho(x) A \ddot{W} - \frac{\partial}{\partial x}(\rho(x) I W_{,xtt}) + (N_T + N_M) w_{,xx} \right] - E(x) I W_{,xx} + l^2 \frac{\partial}{\partial x}(E(x) I W_{,xxx}) \tag{15}$$

The final equation of Euler's beam method is used to study transverse vibration using NSGT as follows:

$$\begin{aligned} &EI\frac{\partial^4 w}{\partial x^4} - l^2 EI\frac{\partial^6 w}{\partial x^6} + \rho A\frac{\partial^2 w}{\partial t^2} - \rho I\frac{\partial^4 w}{\partial x^2 \partial t^2} - (ea)^2 \rho A\frac{\partial^4 w}{\partial x^2 \partial t^2} - (N_T + N_M)\frac{\partial^2 w}{\partial x^2} \\ &+ (ea)^2 (N_T + N_M)\frac{\partial^4 w}{\partial x^4} + (ea)^2 \rho I\frac{\partial^6 w}{\partial x^4 \partial t^2} = 0 \end{aligned} \tag{16}$$

where:

$$N_T = -\lambda_1 h \Delta T \ \& \ N_M = m H_x^2 \frac{\partial^2 w}{\partial x^2} \tag{17}$$

where, H_x & m are in-plane uniaxial magnetic field and the magnetic field permeability. λ_1, h and ΔT demonstrate the coefficient of thermal expansion, the cross-sectional area, and the difference between the temperature and its initial reference temperature.

Assuming [4, 50, 51]:

$$w(x, t) = V(x) e^{i\omega t} \tag{18}$$

Substituting Equation (18) in Equation (17):

$$\begin{aligned} &-l^2 EIV^6(x) + (EI - (ea)^2 \rho I\omega^2 + (ea)^2 (N_T + N_M))V^4(x) + (\rho I\omega^2 + (ea)^2 \rho A\omega^2 \\ &+ (N_T + N_M))V''(x) - \rho A\omega^2 V(x) = 0 \end{aligned} \tag{19}$$

By multiplying the Equation (19) in $\frac{L^4}{EI}$ and by assuming:

$$\bar{V} = \frac{V}{L},\ \xi = \frac{x}{L},\ \alpha_1 = \frac{ea}{L},\ \alpha_2 = \frac{l}{L},\ \lambda^4 = \frac{\rho A L^4 \omega^2}{EI},\ h^2 = \frac{L^2 \rho I \omega^2}{EI},\ \bar{N}_T = \frac{N_T L^2}{EI},\ \bar{N}_M = \frac{N_M L^2}{EI} \tag{20}$$

With combining Equations (20) and (19) results:

$$-\alpha_2^2\bar{V}^6(\xi)+(1-\alpha_1^2h^2+\alpha_1^2(\bar{N}_T+\bar{N}_M))\bar{V}^4(\zeta)+(h^2+\alpha_1^2\lambda^4+(\bar{N}_T+\bar{N}_M))\bar{V}''(\xi)$$
$$-\lambda^4\bar{V}(\xi)=0 \tag{21}$$

To solve Equation (21) with the assumption Equation (22), Equation (23) is obtained [50]:

$$\bar{V}(\xi)=\sum_{k=1}^{6}\bar{V}_k\exp(\eta_k\xi) \tag{22}$$

$$-\alpha_2^2\eta^6+(1-\alpha_1^2h^2+\alpha_1^2(\bar{N}_T+\bar{N}_M))\eta^4+(h^2+\alpha_1^2\lambda^4+(\bar{N}_T+\bar{N}_M))\eta^2-\lambda^4=0 \tag{23}$$

where results in Equation (23), η as follows:

$$\eta_1^2=-\frac{1}{3(-\alpha_2^2)}\left((1-\alpha_1^2h^2+\alpha_1^2(\bar{N}_T+\bar{N}_M))+R+\frac{(1-\alpha_1^2h^2+\alpha_1^2(\bar{N}_T+\bar{N}_M))^2}{R}\right)$$
$$\eta_2^2=-\frac{1}{3(-\alpha_2^2)}\left((1-\alpha_1^2h^2+\alpha_1^2(\bar{N}_T+\bar{N}_M))+\frac{-1-i\sqrt{3}}{2}R+\frac{(1-\alpha_1^2h^2+\alpha_1^2(\bar{N}_T+\bar{N}_M))^2}{\left(\frac{-1-i\sqrt{3}}{2}\right)R}\right) \tag{24}$$
$$\eta_3^2=-\frac{1}{3(-\alpha_2^2)}\left((1-\alpha_1^2h^2+\alpha_1^2(\bar{N}_T+\bar{N}_M))+\frac{-1+i\sqrt{3}}{2}R+\frac{(1-\alpha_1^2h^2+\alpha_1^2(\bar{N}_T+\bar{N}_M))^2}{\left(\frac{-1+i\sqrt{3}}{2}\right)R}\right)$$

where in Equation (24):

$$R=\sqrt[3]{\frac{2(1-\alpha_1^2h^2+\alpha_1^2(\bar{N}_T+\bar{N}_M))^3+\sqrt{-27(-\alpha_2^2)^2\Delta}}{2}}$$
$$\Delta=-4(1-\alpha_1^2h^2+\alpha_1^2(\bar{N}_T+\bar{N}_M))^3(h^2+\alpha_1^2\lambda^4-\lambda^4+(\bar{N}_T+\bar{N}_M)) \tag{25}$$
$$-27(-\alpha_2^2)^2(h^2+\alpha_1^2\lambda^4-\lambda^4+(\bar{N}_T+\bar{N}_M))^2$$

The third root is always negative for physics, and gives imaginary values, so:

$$\bar{V}(\xi)=A_1+A_2\xi+A_3\sinh(\eta_1\xi)+A_4\cosh(\eta_1\xi)+A_5\sin(\eta_2\xi)+A_6\cos(\eta_2\xi) \tag{26}$$

3. Nanobeam crack model

As seen in Figure 1, the nanobeam crack was replaced by an elastic longitudinal spring and a torsional spring [52]. Therefore, strain energy Θ nanobeam is obtained as follows:

$$\Theta = \frac{1}{2}\int_0^L dx \int_A \sigma_{xx}\left(\frac{\partial u}{\partial x} - z\frac{\partial^2 V}{\partial x^2}\right)dA + \Delta\Theta_c \tag{27}$$

where $\Delta\Theta_c$ does the crack cause the additional strain energy. This equation can be expressed as follows, which includes axial force and bending moment [52]:

$$\Theta = \frac{1}{2}\int_0^L \left(N\frac{\partial u}{\partial x} + M\frac{\partial^2 V}{\partial x^2}\right)dx + \Delta\Theta_c \tag{28}$$

The increment due to the presence of an edge crack [52]:

$$\Delta\Theta_c = \frac{1}{2}k_{MM}M(L^k,t)\frac{\partial^2 V}{\partial x^2} + \frac{1}{2}k_{NN}N(L^k,t)\frac{\partial u}{\partial x} + \frac{1}{2}k_{MN}M(L^k,t)\frac{\partial u}{\partial x} + \frac{1}{2}k_{NM}N(L^k,t)\frac{\partial^2 V}{\partial x^2} \tag{29}$$

where k_{MM}, k_{NN}, k_{MN} and k_{NM} are the flexibility constants [52]. The increment of strain energy could be written as:

$$\Delta\Theta_c = \frac{1}{2}M\Delta\theta + \frac{1}{2}N\Delta u \tag{30}$$

where $\Delta\theta$ and Δu are, the angle rotated by the rotational spring and the relative horizontal displacement at the edge crack section. In this paper, cross-sectional vibration is considered, and longitudinal movement is not considered ($\Delta u = 0$). $\Delta\theta$ it can be expressed in this way [52]:

$$\Delta\theta = k_{MM}\frac{\partial^2 V}{\partial x^2} \tag{31}$$

The dimensionless form of Equation (31) is [52]:

$$\Delta\theta = \frac{k_{MM}}{L}\left.\frac{\partial^2 \bar{V}}{\partial x^2}\right|_{\xi=L^c} = k\left.\frac{\partial^2 \bar{V}}{\partial x^2}\right|_{\xi=L^c} \tag{32}$$

The free cross-sectional vibration analysis of the beam can be continued by applying the motion equation in the vertical direction to each of the following two sections:

$$
\begin{aligned}
&-\alpha_2^2\bar{V}^6(\xi)+(1-\alpha_1^2h^2+\alpha_1^2(\bar{N}_T+\bar{N}_M))\bar{V}^4(\zeta)+(h^2+\alpha_1^2\lambda^4+(\bar{N}_T+\bar{N}_M))\bar{V}''(\xi)-\lambda^4\bar{V}(\xi)=0\\
&0\le\xi\le b\\
&-\alpha_2^2\bar{V}^6(\xi)+(1-\alpha_1^2h^2+\alpha_1^2(\bar{N}_T+\bar{N}_M))\bar{V}^4(\zeta)+(h^2+\alpha_1^2\lambda^4+(\bar{N}_T+\bar{N}_M))\bar{V}''(\xi)-\lambda^4\bar{V}(\xi)=0\\
&b\le\xi\le 1
\end{aligned}
\tag{33}
$$

where λ^4 is the natural frequency. The solution for each division can be expressed as follows:

$$
\begin{aligned}
&\bar{V}_1(\xi)=A_1+A_2\xi+A_3\sinh(\eta_1\xi)+A_4\cosh(\eta_1\xi)+A_5\sin(\eta_2\xi)+A_6\cos(\eta_2\xi)\qquad 0\le\xi\le b\\
&\bar{V}_1(\xi)=B_1+B_2\xi+B_3\sinh(\eta_1\xi)+B_4\cosh(\eta_1\xi)+B_5\sin(\eta_2\xi)+B_6\cos(\eta_2\xi)\qquad b\le\xi\le 1
\end{aligned}
\tag{34}
$$

In the following, using the boundary conditions of the beginning, the crack area, and the end of the nanobeam, we have:

$$
\begin{aligned}
&\bar{V}_1(0)=\bar{V}_1''(0)=\bar{V}_1^4(0)=0\\
&\bar{V}_2(1)=\bar{V}_2''(1)=\bar{V}_2^4(1)=0\\
&-\alpha_2^2\bar{V}_2^4(b)+\left(1-\alpha_1^2h^2+\alpha_1^2\left(\bar{N}_T+\bar{N}_M\right)\right)\bar{V}_2''(b)+\left(h^2+\alpha_1^2\lambda^4\right)\bar{V}_2(b)\\
=&-\alpha_2^2\bar{V}_1^4(b)+\left(1-\alpha_1^2h^2+\alpha_1^2\left(\bar{N}_T+\bar{N}_M\right)\right)\bar{V}_1''(b)+\left(h^2+\alpha_1^2\lambda^4\right)\bar{V}_1(b)\\
&\bar{V}_2'(b)-\bar{V}_1'(b)=k\bar{V}_1''(b)\\
&-\alpha_2^2\bar{V}_2''(b)+\left(1-\alpha_1^2h^2+\alpha_1^2\left(\bar{N}_T+\bar{N}_M\right)\right)\bar{V}_2(b)\\
=&-\alpha_2^2\bar{V}_1''(b)+\left(1-\alpha_1^2h^2+\alpha_1^2\left(\bar{N}_T+\bar{N}_M\right)\right)\bar{V}_1(b)\\
&-\alpha_2^2\bar{V}_2^5(b)+\left(1-\alpha_1^2h^2+\alpha_1^2\left(\bar{N}_T+\bar{N}_M\right)\right)\bar{V}_2^3(b)+\left(h^2+\alpha_1^2\lambda^4\right)\bar{V}_2'(b)\\
=&-\alpha_2^2\bar{V}_1^5(b)+\left(1-\alpha_1^2h^2+\alpha_1^2\left(\bar{N}_T+\bar{N}_M\right)\right)\bar{V}_1^3(b)+\left(h^2+\alpha_1^2\lambda^4\right)\bar{V}_1'(b)
\end{aligned}
\tag{35}
$$

The natural frequencies are obtained by applying the boundary conditions in Equation (34) and forming the matrix of coefficients.

4. Results and discussion

The previous sections show that the nanobeam Euler-Bernoulli equations were derived using the strain gradient theory and Hamilton's principle. This section obtains the results for various parameters, including crack area, temperature, magnetism, and spring stiffness changes that greatly impact dimensionless natural frequencies. The results are compared with Loya et al. [52]. It is presented in Table 1.

Where:

$$\frac{L}{h} = 100, \quad B = 10h$$

Table 1. Comparison of the first four frequencies with $\alpha_1 = \alpha_2 = 0$, $b = 0.25$

$k = 2$		$k = 0.35$		$k = 0.065$		$k = 0$		Ω
Present	[52]	Present	[52]	Present	[52]	Present	[52]	
2.3493	2.3493	2.9071	2.9071	3.0921	3.0921	3.1416	3.1416	1
5.1047	5.1047	5.6491	5.6491	6.1028	6.1028	6.2832	6.2832	2
8.9008	8.9008	9.0767	9.0767	9.3021	9.3021	9.4248	9.4248	3
12.5664	12.5664	12.5664	12.5664	12.5664	12.5664	12.5664	12.5664	4

In the following (Table 2-5), the first and second dimensionless frequencies have been used for different values of thermal and magnetic.

Table 2. Temperature change ΔT (°C) on the first frequencies with $\alpha_1 = 0.4$, $\alpha_2 = 0.2$, $b = 0.25$, $m = 0$

k	$\Delta T = 0$	$\Delta T = 20$	$\Delta T = 40$	$\Delta T = 60$	$\Delta T = 80$	$\Delta T = 100$
0.065	3.63812	3.62412	3.61802	3.60792	3.59772	3.58752
0.35	3.47242	3.46241	3.45232	3.44221	3.43202	3.42182
2	2.96542	2.95540	2.94531	2.93522	2.92502	2.91482

Table 3. Temperature change ΔT (°C) on the first frequencies with $\alpha_1 = 0.4$, $\alpha_2 = 0.2$, $b = 0.5$, $m = 0$

k	$\Delta T = 0$	$\Delta T = 20$	$\Delta T = 40$	$\Delta T = 60$	$\Delta T = 80$	$\Delta T = 100$
0.065	3.50717	3.49718	3.48707	3.47697	3.46677	3.45656
0.35	3.26065	3.25065	3.24055	3.23045	3.22025	3.21005
2	2.72345	2.71344	2.70335	2.69325	2.68301	2.67286

Table 4. Temperature change ΔT (°C) on the second frequencies with $\alpha_1 = 0.4$, $\alpha_2 = 0.2$, $b = 0.25$, $m = 0$

k	$\Delta T = 0$	$\Delta T = 20$	$\Delta T = 40$	$\Delta T = 60$	$\Delta T = 80$	$\Delta T = 100$
0.065	4.65679	4.62719	4.59759	4.56779	4.53809	4.50819
0.35	4.49109	4.46149	4.43189	4.0209	4.37239	4.34248
2	3.98409	3.95444	3.92488	3.89501	3.86539	3.83545

Table 5. Temperature change ΔT (°C) on the second frequencies with $\alpha_1 = 0.4$, $\alpha_2 = 0.2$, $b = 0.5$, $m = 0$

k	$\Delta T = 0$	$\Delta T = 20$	$\Delta T = 40$	$\Delta T = 60$	$\Delta T = 80$	$\Delta T = 100$
0.065	4.80232	4.77272	4.74312	4.71331	4.68361	4.65372
0.35	4.55582	4.52622	4.49662	4.46683	4.43711	4.40722
2	4.55582	4.52622	4.49662	4.46683	4.43711	4.40722

Tables 2 and 4 show the effects of temperature and spring stiffness changes on the first and second dimensionless frequency $\alpha_1 = 0.4$, $\alpha_2 = 0.2$, $b = 0.25$, $m = 0$.

As can be seen, the dimensionless natural frequency decreases with increasing temperature. The effects of temperature cause changes in the stiffness of the nanobeam. In this study, the intensity of the crack zone was simulated with two torsional and longitudinal springs. The increase in crack growth severity is applied by increasing the torsional and longitudinal spring stiffness; as can be seen, with increasing values of k, the dimensionless natural frequency decreases, which is caused by the decrease in the strength of the nanobeam.

Tables 3 and 5 also show temperature changes for the first and second dimensionless frequencies. The important difference between these two tables is the change in the crack area (b), which has been moved from $b = 0.25$ to $b = 0.5$.

The dimensionless natural frequency decreases by moving the crack region to the middle of the nanobeam, which is again due to the changes in the stiffness of the nanobeam and the same strength of the nanobeam.

Tables 2-5 observed the effects of temperature on the first and second dimensionless natural frequencies. This temperature increase until reaching the critical temperature causes a decrease in the natural frequency; until finally reaching the critical temperature, the frequency reaches zero.

Table 6. The effect of the magnetic change (m) on the first frequencies with $\alpha_1 = 0.4$, $\alpha_2 = 0.2$, $b = 0.25$, $\Delta T = 0$

k	$m = 0$	$m = 10$	$m = 20$	$m = 30$	$m = 50$	$m = 100$
0.065	3.63812	3.65811	3.68812	3.72810	3.75811	3.94812
0.35	3.47242	3.49242	3.52240	3.56148	3.59339	3.78149
2	2.96542	2.98498	3.01538	3.05540	3.08541	3.27492

Table 7. The effect of the magnetic change (m) on the first frequencies with $\alpha_1 = 0.4$, $\alpha_2 = 0.2$, $b = 0.5$, $\Delta T = 0$

k	$m = 0$	$m = 10$	$m = 20$	$m = 30$	$m = 50$	$m = 100$
0.065	3.50717	3.52717	3.55713	3.59711	3.62717	3.1716
0.35	3.26065	3.28060	3.31058	3.35057	3.38071	3.57079
2	2.72345	2.74340	2.77338	2.81345	2.84350	3.03359

Table 8. The effect of the magnetic change (m) on the second frequencies with $\alpha_1 = 0.4$, $\alpha_2 = 0.2$, $b = 0.25$, $\Delta T = 0$

k	$m = 0$	$m = 10$	$m = 20$	$m = 30$	$m = 50$	$m = 100$
0.065	4.65679	4.68677	4.71678	4.75680	4.86681	5.04671
0.35	4.49109	4.52101	4.55110	4.59113	4.70109	4.88100
2	3.98409	4.01408	4.04407	4.08412	4.19415	4.37400

Table 9. The effect of the magnetic change (m) on the second frequencies with $\alpha_1 = 0.4$, $\alpha_2 = 0.2$, $b = 0.5$, $\Delta T = 0$

k	$m = 0$	$m = 10$	$m = 20$	$m = 30$	$m = 50$	$m = 100$
0.065	4.80232	4.83232	4.86228	4.90226	5.01230	5.19235
0.35	4.55582	4.58581	4.61580	4.65588	4.76590	4.94579
2	4.55582	4.58581	4.61580	4.65588	4.76590	4.94579

Tables 6-9 show the effects of applying the magnetic environment on the nanobeam's first and second dimensionless natural frequencies. In this case, there is no temperature environment. Most of the interpretations of Tables 2-5 apply to these tables. As can be seen, increasing the magnetization has caused an increase in the first and second dimensionless natural frequencies.

Changes in magnetization cause changes in nanobeam stiffness. Such temperature and magnetism show their effects on the equations' stress results.

By choosing the appropriate parameters, the vibration behavior can be controlled, and the stability of the structure can be increased.

As seen in Figures 2 and 3, the effects of temperature and magnetism on the dimensionless natural frequency are shown. As the temperature increases, the dimensionless natural frequency should decrease. As the magnetization increases, the dimensionless natural frequency increases.

These two Figures important points are as the crack region nanobeam from the beginning of the nanobeam to the end of the nanobeam; first, the frequency decreases, then in the middle of the nanobeam ($b = 0.5$), this frequency reduction process reaches its peak and passing through the middle of the nanobeam, the dimensionless frequency increase. The middle of the nanobeam acts like a mirror, and the amount of frequency changes before and after it is the same in certain areas of the crack. Which well shows the strength of the nanobeam in different areas of the crack, which causes changes in the dimensionless frequency.

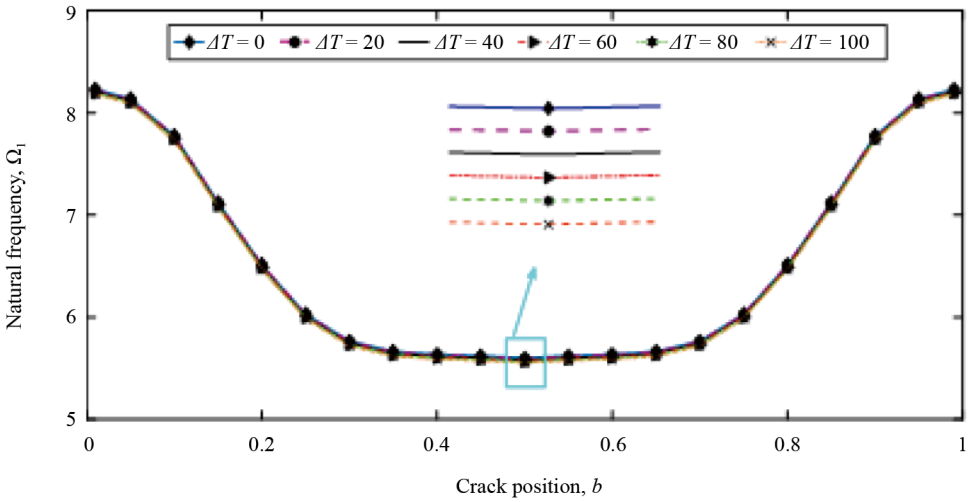

Figure 2. Thermal effects for diverse crack severity $\alpha_1 = 0.2$, $\alpha_2 = 0.6$, $k = 0.065$ on the first dimensionless natural frequency

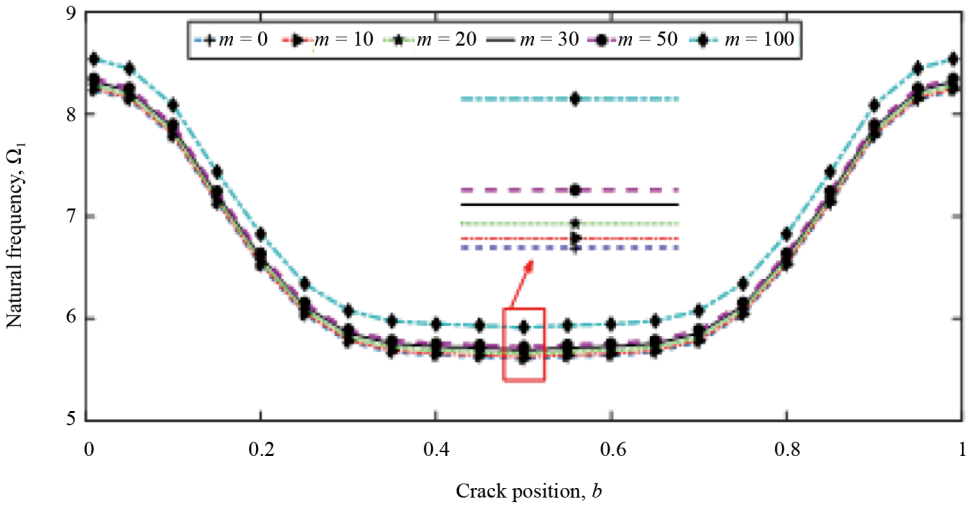

Figure 3. Magnetic effects for diverse crack severity $\alpha_1 = 0.2$, $\alpha_2 = 0.6$, $k = 0.065$ on the first dimensionless natural frequency

In the presence of a magnetic field, certain materials may experience changes in their physical properties. This phenomenon is known as the magnetostrictive effect. When subjected to a magnetic field, magnetostrictive materials undergo a change in shape or size. In the case of the nanobeam crystalline structure, the magnetic field causes the material to contract.

The contraction of the nanobeam crystalline structure leads to an increase in its stiffness. Stiffness refers to the resistance of a material to deformation under an applied load. When a material becomes stiffer, its natural frequencies tend to increase. Natural frequencies are the inherent frequencies at which an object or structure tends to vibrate when excited.

Therefore, as the magnetic values increase and the nanobeam crystalline structure contracts, the stiffness of the structure increases, resulting in higher dimensionless natural frequencies.

5. Conclusions

In this paper, an Euler-Bernoulli nanobeam that has been weakened by considering a crack in the magnetic and thermal environment was investigated. First, the equations of motion were obtained using Hamilton's principle; then, the crack region was modeled with two torsional and longitudinal springs. The strain energy of the nanobeam with crack conditions was defined, and a general solution was presented. Twelve different boundary conditions were extracted for the beginning, the crack area, and the end of the nanobeam to obtain the natural frequencies by forming a matrix of coefficients.

In the following, the influencing parameters on the analysis of nanobeam vibrations, including magnetism, temperature, crack area and crack growth intensity, were investigated. It was found that with the increase in temperature, the natural dimensionless frequency should decrease, and with the increase in magnetism, the natural dimensionless frequency increases. The effects of temperature and magnetism are on the results of stress, which increases or decreases the stiffness of the nanobeam. With the increase in the intensity of the crack, which is shown in this article with the k parameter, the natural frequency decreases due to the decrease in the strength of the nanobeam, which ultimately leads to changes in the stiffness of the nanobeam. Finally, the dimensionless natural frequency decreases by changing the crack area towards the middle of the nanobeam. As the crack area moves from the beginning of the nanobeam to the middle of the nanobeam, the frequency decreases and then acts proportionally; as the crack area moves towards the end of the nanobeam, the dimensionless natural frequency increases. With the appropriate selection of these influencing factors on the vibration behavior of the nanobeam, the strength of the desired structure can be increased.

Conflict of interest

The authors declare no competing financial interest.

References

[1] Eghbali M, Hosseini SA, Pourseifi M. An dynamical evaluation of size-dependent weakened nano-beam based on the nonlocal strain gradient theory. *The Journal of Strain Analysis for Engineering Design*. 2023; 58(5): 357-366.

[2] Eghbali M, Hosseini SA. On moving harmonic load and dynamic response of carbon nanotube-reinforced composite beams using higher-order shear deformation theories. *Mechanics of Advanced Composite Structures*. 2023; 10(2): 257-270.

[3] Jafarpour V, Abasi M. Optimization of load values in pipe hydroforming process using a fuzzy load control algorithm. *Journal of Brilliant Engineering*. 2022; 3: 4683.

[4] Eghbali M, Hosseini SA, Pourseifi M. Free transverse vibrations analysis of size-dependent cracked piezoelectric nano-beam based on the strain gradient theory under mechanic-electro forces. *Engineering Analysis with Boundary Elements*. 2022; 143: 606-612.

[5] Eghbali M, Hosseini SA, Hamidi BA. Mantari's higher-order shear deformation theory of sandwich beam with CNTRC face layers with porous core under thermal loading. *International Journal of Structural Stability and Dynamics*. 2022; 22(16): 2250181.

[6] Eghbali M, Hosseini SA. Influences of magnetic environment and two moving loads on lateral and axial displacement of sandwich graphene-reinforced copper-based composite beams with soft porous core. *Journal of Vibration and Control*. 2022; 29(23-24): 5373-5386.

[7] Eghbali M, Hosseini SA, Rahmani O. Free vibration of axially functionally graded nanobeam with an attached mass based on nonlocal strain gradient theory via new ADM numerical method. *Amirkabir Journal of Mechanical Engineering*. 2021; 53(2): 1-8.

[8] Wang S, Kang W, Yang W, Zhang Z, Li Q, Liu M, et al. Hygrothermal effects on buckling behaviors of porous bi-directional functionally graded micro-/nanobeams using two-phase local/nonlocal strain gradient theory. *European Journal of Mechanics-A/Solids*. 2022; 94: 104554.

[9] Thai CH, Nguyen-Xuan H, Phung-Van P. A size-dependent isogeometric analysis of laminated composite plates based on the nonlocal strain gradient theory. *Engineering with Computers*. 2022; 39: 331-345.
[10] Malikan M, Krasheninnikov M, Eremeyev VA. Torsional stability capacity of a nano-composite shell based on a nonlocal strain gradient shell model under a three-dimensional magnetic field. *International Journal of Engineering Science*. 2020; 148: 103210.
[11] Merzouki T, Ahmed HMS, Bessaim A, Merzouki T, Dimitri R, Tornabene F, et al. Bending analysis of functionally graded porous nanocomposite beams based on a non-local strain gradient theory. *Mathematics and Mechanics of Solids*. 2022; 27(1): 66-92.
[12] Tho NC, Thanh NT, Tho TD, Van Minh P, Hoa LK. Modelling of the flexoelectric effect on rotating nanobeams with geometrical imperfection. *Journal of the Brazilian Society of Mechanical Sciences and Engineering*. 2021; 43: 1-22.
[13] Duc DH, Van Minh P, Tung NS. Finite element modelling for free vibration response of cracked stiffened FGM plates. *Vietnam Journal of Science and Technology*. 2020; 58(1): 119-129.
[14] Dung NT, Van Ke T, Huyen TTH, Thai LM, Minh PV. Nonlinear static bending analysis of microplates resting on imperfect two-parameter elastic foundations using modified couple stress theory. *Comptes Rendus. Mécanique*. 2022; 350(G1): 121-141.
[15] Tho NC, Cong PH, Zenkour AM, Doan DH, Van Minh P. Finite element modeling of the bending and vibration behavior of three-layer composite plates with a crack in the core layer. *Composite Structures*. 2023; 305: 116529.
[16] Khan NS, Shah Q, Sohail A, Kumam P, Thounthong P, Muhammad T. Mechanical aspects of Maxwell nanofluid in dynamic system with irreversible analysis. *ZAMM-Journal of Applied Mathematics and Mechanics/Zeitschrift für Angewandte Mathematik und Mechanik*. 2021; 101(12): e202000212.
[17] Ramzan M, Khan NS, Kumam P. Mechanical analysis of non-Newtonian nanofluid past a thin needle with dipole effect and entropic characteristics. *Scientific Reports*. 2021; 11(1): 19378.
[18] Khan NS, Kumam P, Thounthong P. Magnetic field promoted irreversible process of water based nanocomposites with heat and mass transfer flow. *Scientific Reports*. 2021; 11(1): 1692.
[19] Li S, Chi W. Nonlinear impact on the buckling characteristic of functionally graded nonlocal nanotube via a couple of nonlocal strain gradient theory and a novel higher-order tube theory. *Waves in Random and Complex Media*. 2022; 2022: 2026530. Available from: https://doi.org/10.1080/17455030.2022.2026530.
[20] Malikan M, Nguyen VB. Buckling analysis of piezo-magnetoelectric nanoplates in hygrothermal environment based on a novel one variable plate theory combining with higher-order nonlocal strain gradient theory. *Physica E: Low-Dimensional Systems and Nanostructures*. 2018; 102: 8-28.
[21] Forooghi A, Alibeigloo A. Hygro-thermo-magnetically induced vibration of FG-CNTRC small-scale plate incorporating nonlocality and strain gradient size dependency. *Waves in Random and Complex Media*. 2022; 2022: 2037784. Available from: https://doi.org/10.1080/17455030.2022.2037784.
[22] Khan NS, Usman AH, Sohail A, Shah A, Hussanan Q, Ullah N, et al. A framework for the magnetic dipole effect on the thixotropic nanofluid flow past a continuous curved stretched surface. *Crystals*. 2021; 11(6): 645.
[23] Eftekhari SA, Toghraie D. Vibration and dynamic analysis of a cantilever sandwich microbeam integrated with piezoelectric layers based on strain gradient theory and surface effects. *Applied Mathematics and Computation*. 2022; 419: 126867.
[24] Malikan M, Nguyen VB, Tornabene F. Damped forced vibration analysis of single-walled carbon nanotubes resting on viscoelastic foundation in thermal environment using nonlocal strain gradient theory. *Engineering Science and Technology, an International Journal*. 2018; 21(4): 778-786.
[25] Khan NS, Humphries UW, Kumam W, Kumam P, Muhammad T. Assessment of irreversibility optimization in Casson nanofluid flow with leading edge accretion or ablation. *ZAMM-Journal of Applied Mathematics and Mechanics/Zeitschrift für Angewandte Mathematik und Mechanik*. 2022; 102(10): e202000207.
[26] Rajaei A, Chizfahm A, Vatankhah R, Montazeri A. Adaptive self-organizing fuzzy sliding mode controller for a nonlocal strain gradient nanobeam. *European Journal of Control*. 2022; 65: 100626.
[27] Mohammadian M, Hosseini SM. A size-dependent differential quadrature element model for vibration analysis of FG CNT reinforced composite microrods based on the higher order Love-Bishop rod model and the nonlocal strain gradient theory. *Engineering Analysis with Boundary Elements*. 2022; 138: 235-252.

[28] Thanh C-L, Nguyen KD, Minh H-L, Thanh S-T, Phuong P-V, Wahab MA. Nonlocal strain gradient IGA numerical solution for static bending, free vibration and buckling of sigmoid FG sandwich nanoplate. *Physica B: Condensed Matter*. 2022; 631: 413726.

[29] Malikan M, Nguyen VB, Dimitri R, Tornabene F. Dynamic modeling of non-cylindrical curved viscoelastic single-walled carbon nanotubes based on the second gradient theory. *Materials Research Express*. 2019; 6(7): 075041.

[30] Khan NS, Fernandez-Gamiz U, Khan MS, Kumam W, Kumam P, Galal A. Thermodynamics of second-grade nanofluid over a stretchable rotating porous disk subject to Hall current and cubic autocatalysis chemical reactions. *Frontiers in Physics*. 2022; 10: 961774.

[31] Yang W, Wang S, Kang W, Yu T, Li Y. A unified high-order model for size-dependent vibration of nanobeam based on nonlocal strain/stress gradient elasticity with surface effect. *International Journal of Engineering Science*. 2023; 182: 103785.

[32] Qing H, Tang Y. Size-dependent fracture analysis of Centrally-Cracked nanobeam using Stress-Driven Two-Phase Local/Nonlocal integral model with discontinuity and symmetrical conditions. *Engineering Fracture Mechanics*. 2023; 282: 109193.

[33] Barretta R, Caporale A, Luciano R, Vaccaro MS. Nonlocal gradient mechanics of nanobeams for non-smooth fields. *International Journal of Engineering Science*. 2023; 189: 103879.

[34] Scorza D, Vantadori S, Luciano R. Nanobeams with internal discontinuities: A local/nonlocal approach. *Nanomaterials*. 2021; 11(10): 2651.

[35] Khan NS, Sriyab S, Kaewkhao A, Thawinan E. Hall current effect in bioconvection Oldroyd-B nanofluid flow through a porous medium with Cattaneo-Christov heat and mass flux theory. *Scientific Reports*. 2022; 12(1): 19821.

[36] Su J, Qu Y, Zhang K, Zhang Q, Tian Y. Vibration analysis of functionally graded porous piezoelectric deep curved beams resting on discrete elastic supports. *Thin-Walled Structures*. 2021; 164: 107838.

[37] Arefi M, Pourjamshidian M, Ghorbanpour Arani A, Rabczuk T. Influence of flexoelectric, small-scale, surface and residual stress on the nonlinear vibration of sigmoid, exponential and power-law FG Timoshenko nano-beams. *Journal of Low Frequency Noise, Vibration and Active Control*. 2019; 38(1): 122-142.

[38] Malikan M, Nguyen VB, Tornabene F. Electromagnetic forced vibrations of composite nanoplates using nonlocal strain gradient theory. *Materials Research Express*. 2018; 5(7): 075031.

[39] Darban H, Luciano R, Basista M. Free transverse vibrations of nanobeams with multiple cracks. *International Journal of Engineering Science*. 2022; 177: 103703.

[40] Khan NS, Hussanan A, Kumam W, Kumam P, Suttiarporn P. Accessing the thermodynamics of Walter-B fluid with magnetic dipole effect past a curved stretching surface. *ZAMM-Journal of Applied Mathematics and Mechanics/Zeitschrift für Angewandte Mathematik und Mechanik*. 2023; 103(8): e202100112.

[41] Bouafia K, Kaci A, Houari MSA, Benzair A, Tounsi A. A nonlocal quasi-3D theory for bending and free flexural vibration behaviors of functionally graded nanobeams. *Smart Structures and Systems*. 2017; 19(2): 115-126.

[42] Yahia SA, Atmane HA, Houari MSA, Tounsi A. Wave propagation in functionally graded plates with porosities using various higher-order shear deformation plate theories. *Structural Engineering and Mechanics*. 2015; 53(6): 1143-1165.

[43] Malikan M, Eremeyev VA, Żur KK. Effect of axial porosities on flexomagnetic response of in-plane compressed piezomagnetic nanobeams. *Symmetry*. 2020; 12(12): 1935.

[44] Karami B, Shahsavari D, Janghorban M, Li L. On the resonance of functionally graded nanoplates using bi-Helmholtz nonlocal strain gradient theory. *International Journal of Engineering Science*. 2019; 144: 103143.

[45] Chaht FL, Kaci A, Houari MSA, Tounsi A. Bending and buckling analyses of functionally graded material (FGM) size-dependent nanoscale beams including the thickness stretching effect. *Steel and Composite Structures*. 2015; 18(2): 425-442.

[46] Belkorissat I, Houari MSA, Tounsi A, Adda Bedia EA, Mahmoud SR. On vibration properties of functionally graded nano-plate using a new nonlocal refined four variable model. *Steel and Composite Structures*. 2015; 18(4): 1063-1081.

[47] Eringen AC. On differential equations of nonlocal elasticity and solutions of screw dislocation and surface waves. *Journal of Applied Physics*. 1983; 54(9): 4703-4710.

[48] Lim C, Zhang G, Reddy J. A higher-order nonlocal elasticity and strain gradient theory and its applications in wave propagation. *Journal of the Mechanics and Physics of Solids*. 2015; 78: 298-313.

[49] Eghbali M, Hosseini SA, Rahmani O. Free vibration of axially functionally graded nanobeam with an attached mass based on nonlocal strain gradient theory via new ADM numerical method. *Amirkabir Journal of Mechanical Engineering*. 2021; 53(2): 8.
[50] Sourki R, Hoseini S. Free vibration analysis of size-dependent cracked microbeam based on the modified couple stress theory. *Applied Physics A*. 2016; 122(4): 1-11.
[51] Eghbali M, Hosseini SA, Hamidi BA. Mantari's higher-order shear deformation theory of sandwich beam with CNTRC face layers with porous core under thermal loading. *International Journal of Structural Stability and Dynamics*. 2022; 22(16): 2250181.
[52] Loya J, López-Puente J, Zaera R, Fernández-Sáez J. Free transverse vibrations of cracked nanobeams using a nonlocal elasticity model. *Journal of Applied Physics*. 2009; 105(4): 044309.